International Journal of Modern Physics B, Vol. 14, No. 17 (2000) 1801–1813

BIFURCATION STRUCTURE OF THE DOUBLE-WELL DUFFING OSCILLATOR

SANG-YOON KIM*

Department of Physics, Kangwon National University
Chunchon, Kangwon-Do 200-701, Korea

Received 24 April 2000
Revised 29 June 2000

We consider a forced Duffing oscillator with a double-well potential, which behaves as an asymmetric soft oscillator in each potential well. Bifurcations associated with resonances of the asymmetric attracting periodic orbits, arising from the two stable equilibrium points of the potential, are investigated in details by varying the two parameters A (the driving amplitude) and ω (the driving frequency). We thus obtain the phase diagram showing rich bifurcation structure in the ω–A plane. For the subharmonic resonances, the corresponding period-doubling bifurcation curves become folded back, within which diverse bifurcation phenomena such as "period bubblings" are observed. For the primary and superharmonic resonances, the corresponding saddle-node bifurcation curves form "horns", leaning to the lower frequencies. With decreasing ω, resonance horns with successively increasing torsion numbers recur in a similar shape. We note that recurrence of self-similar resonance horns is a "universal" feature in the bifurcation structure of many driven nonlinear oscillators.

1. Introduction

A periodically driven double-well Duffing oscillator,[1–3] which has become a classic model for analysis of nonlinear phenomena, is investigated. It can be described in a normalized form by a second-order nonautonomous ordinary differential equations,

$$\ddot{x} + \gamma\dot{x} - x + x^3 = A\cos\omega t\,, \tag{1}$$

where γ is the damping coefficient, and $A\cos\omega t$ is a driving force with amplitude A and frequency ω, and the overdot denotes a differentiation with respect to time t.

The Duffing equation (1) with negative linear stiffness describes the dynamics of a buckled beam[4–6] as well as a plasma oscillator.[7] Its dynamics has been analyzed in great details by Holmes using both the theoretical techniques and the computer simulations.[4] The results of this work have been also confirmed in experiments by Moon.[5,6] Since then, a number of authors have studied the forced double-well Duffing oscillator in the past two decades. Thus, albeit simple looking,

*E-mail: sykim@cc.kangwon.ac.kr

rich dynamical behaviors have been found, including the fractal basin boundaries between coexisting competing attractors,[8] period-doubling transitions to chaos,[9–14] hopping cross-well chaotic states induced through attractor-merging crises or intermittencies,[10–14] hysterisis jumps,[12–14] sudden disappearance of chaotic attractors through crises,[12–14] and a recurring structure of resonances of large symmetric orbits and a regular window structure inside a resonance.[15,16]

In this paper, we investigate the bifurcation behaviors of the forced double-well Duffing oscillator by varying the two parameters A and ω. For the unforced case of $A = 0$, there are two stable equilibrium points at $(x, \dot{x}) = (\pm 1, 0)$. However, as A is increased from 0, a conjugate pair of asymmetric attracting orbits with period $2\pi/\omega$ (fixed points for the Poincaré map) arises from the "unforced" equilibrium points. We are particularly interested in the bifurcations associated with stability of the two asymmetric fixed points of the Poincaré map. So far, only some partial results on such bifurcations have been obtained in a particular region of the parameter plane.[9,12–14] Here we make a global and detailed investigation of the bifurcations associated with resonances of the two asymmetric fixed points to improve our understanding of the bifurcation behaviors of the forced double-well Duffing oscillator.

This paper is organized as follows. In Sec. 2, we discuss characterization of local bifurcations of asymmetric periodic orbits. Bifurcations associated with resonances of the asymmetric attracting periodic orbits, arising from the two stable equilibrium points of the potential, are then investigated through numerical calculations of the Floquet (stability) multipliers[17] and torsion numbers,[18] characterizng the topological property of the local flow, in Sec. 3. We thus obtain the phase diagram showing rich bifurcation structure in the parameter plane. For the subharmonic resonances, the associated period-doubling bifurcation curves are folded, along which there are subcritical and supercritical parts. Diverse bifurcation phenomena such as "period bubblings" are also observed inside the folded bifurcation curve. For the primary and superharmonic resonances, the associated saddle-node bifrucation curves form "horns", and they lean to the lower frequencies, because the double-well Duffing oscillator shows soft spring behavior in each potential well. As ω is decreased, resonance horns with successively increasing torsion numbers and asymptotically "self-similar" shapes appear in the parameter plane, as in many other driven oscillators such as the Toda[19] and Morse[20] oscillators (asymmetric soft oscillators), the pendulum[21] (symmetric soft oscillator), and the single-well Duffing oscillator (symmetric hard oscillator).[22] It is thus suggested that recurrence of self-similar resonance horns be a "universal" feature in the bifurcation structure of many driven nonlinear oscillators.[23] Finally, a summary is given in Sec. 4.

2. Characterization of Local Bifurcations

For the numerical calculations we transform the second-order ordinary differential equation (1) into a system of two first-order ordinary differential equations:

$$\dot{x} = y\,, \tag{2a}$$

$$\dot{y} = f(x, y, t) = -\gamma y + x - x^3 + A\cos\omega t\,. \tag{2b}$$

These equations have a symmetry S, because the transformation

$$S : x \to -x\,, \qquad y \to -y\,, \qquad t \to t + \frac{T}{2} \quad \left[T(\text{period}) = \frac{2\pi}{\omega}\right], \tag{3}$$

leaves Eq. (2) invariant. If an orbit $z(t)[\equiv (x(t), y(t))]$ is invariant under S, it is called a symmetric orbit. Otherwise, it is called an asymmetric orbit and has its "conjugate" orbit $Sz(t)$. Here we consider only the asymmetric orbits.

For the unforced case of $A = 0$, there exists a conjugate pair of stable equilibrium points at $(x, y) = (\pm 1, 0)$. However, as A is increased from 0, two asymmetric attracting orbits with the same period $2\pi\omega$ arise from the "unforced" equilibrium points. We note that they become the asymmetric fixed points of the Poincaré map P, generated by stroboscopically sampling the orbit points with the external driving period T. Hereafter, we will denote the asymmetric fixed points by z_a^*. As an example see Fig. 1 showing the phase portraits of the asymmetric periodic orbits, encircling the two unforced equilibrium points. Linearizing Eq. (2) at $(x, y) = (\pm 1, 0)$, we find that the (unforced and undamped) natural frequency ω_0 is $\sqrt{2}$. Moving out, the orbits surrounding $(\pm 1, 0)$ have successively longer periods. Hence the double-well Duffing oscillator near $(\pm 1, 0)$ behaves as an asymmetric soft spring. For the primary ($n = 1$) and superharmonic ($n = 2, 3, \ldots$) resonances at $\omega \simeq \omega_0/n$ ($\omega_0 = \sqrt{2}$), jump phenomena occur, in which the small asymmetric orbits z_a^* are replaced by relatively large asymmetric orbits. On the other hand, for $\omega \simeq 2\omega_0/n$ ($n = 1, 3, 5, \ldots$) the asymmetric fixed points z_a^* become unstable through the first

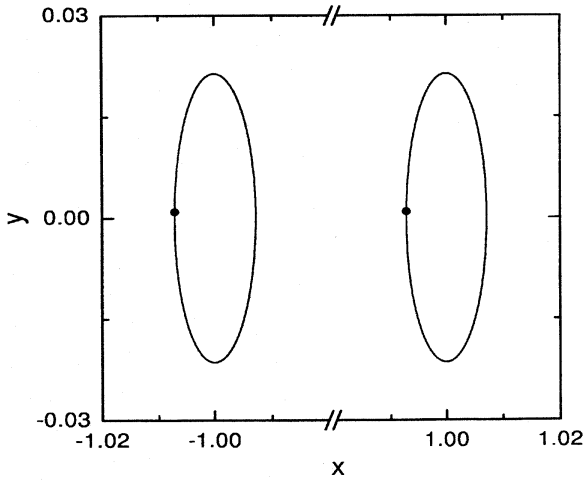

Fig. 1. Phase portrait of two asymmetric attracting orbits with the period $2\pi/\omega$, arising from the two stable equilibrium points of the potential, for $\gamma = 0.1$, $\omega = 3.0$, and $A = 0.05$. The phase flows of the stable asymmetric orbits are denoted by solid curves, and their Poincaré maps are represented by solid circles.

($n = 1$) and secondary ($n = 3, 5, \ldots$) subharmonic resonances. Here we study bifurcations associated with resonances of the asymmetric fixed points z_a^*.

Linear stability of an asymmetric orbit with period q is determined by the eigenvalues, called the Floquet (stability) multipliers, of the linearized Poincaré map DP^q of the q-times iterated map P^q, which can be obtained using the Floquet theory.[17] Using the Liouville's formula,[24] one can easily show that the linearized map DP^q has a constant determinant, $\det DP^q = e^{-\gamma q T}$. Hence the pair of Floquet multipliers of an asymmetric orbit with period q lies either on the circle of radius $e^{-\gamma q T/2}$ or on the real axis in the complex plane. The asymmetric orbit is stable when both Floquet multipliers lie inside the unit circle. We first note that they never cross the unit circle, except at the real axis and hence Hopf bifurcations do not occur. Consequently, a stable asymmetric periodic orbit can lose its stability when a Floquet multiplier passes through 1 or -1 on the real axis. When a Floquet multiplier passes through -1, the stable asymmetric periodic orbit becomes unstable via a supercritical or subcritical period-doubling (PD) bifurcation. On the other hand, when a Floquet multiplier passes through 1, a saddle-node (SN) bifurcation occurs, where the stable asymmetric orbit disappears through collision with an asymmetric unstable orbit with the same period q. For more details on bifurcations, refer to Ref. 25.

There exist many bifurcation curves with the same type (PD or SN) and period in the parameter plane. For a better distinction and classification, we characterize each bifurcation not only by the type and period q, but also by another invariant, the so-called torsion number p, which counts the average rotation number of the nearby orbits during the period q.[18] The torsion number (normalized by the factor 2π) at the SN bifurcation curves becomes an integer. However, when crossing a PD bifurcation curve, not only the period but also the torsion number doubles from an odd multiple of $1/2$ to an odd integer.

Thus our notation for a bifurcation curve, which will be used in Sec. 3, is SN(p, q) for a period-q SN bifurcation with torsion number p and PD(p, q) for a PD bifurcation from period $q/2$ to period q with torsion number p. We choose the pair of (p, q) for the PD bifurcation curve as that of the period-doubled orbit to keep p as an integer.

3. Rich Bifurcation Structure

By varying the two parameters A and ω, we study the bifurcation behaviors, associated with resonances of the asymmetric fixed points z_a^*, arising from the two stable equilibrium points of the potential, for a moderately damped case of $\gamma = 0.1$. We determine the stability of the asymmetric fixed points z_a^* in the $\omega - A$ plane through numerical calculations of the Floquet multipliers and then investigate the bifurcations at the stability boundary curves in details. The torsion numbers of the asymmetric fixed points z_a^* at the bifurcation curves are also obtained to characterize their topological properties. Rich bifurcation behaviors are thus found, as will be seen below.

3.1. *Bifurcation structure associated with the subharmonic resonance*

For $\omega \simeq 2\omega_0$ [$\omega_0 = \sqrt{2}$], a subharmonic resonance occurs in which the asymmetric fixed points z_a^* become unstable by a PD bifurcation. Figure 2 shows the bifurcation structure associated with the subharmonic resonance. We note that the PD(1, 2) bifurcation curve, corresponding to the first subharmonic resonance, becomes folded back at a frequency ω_f ($\simeq 3.23$). This is in contrast to the case of the Toda and Morse oscillators. When crossing the lower part of the folded curve, the asymmetric fixed points z_a^* become unstable through the PD bifurcations. However, when crossing the upper part, they become restabilized through the reverse PD bifurcations. Hence the restabilization of the asymmetric fixed points z_a^* is one characteristic feature for the double-well Duffing oscillator.

The PD bifurcation curves with higher period $q = 4, 8$ are also given in Fig. 2. They correspond to the beginning of two PD cascades. A sequence of bifurcation curves in each PD cascade are characterized by a sequence of pairs (p_n, q_n) which obey a simple relation,[26]

$$p_n = 2^n p_0 \pm \frac{1}{3}[2^n - (-1)^n], \qquad q_n = 2^n q_0 \quad (n = 0, 1, 2, \ldots). \tag{4}$$

where p_0 (= 1) and q_0 (= 2) are the basic torsion number and period, respectively. Both choices of sign are realized by following the two different PD routes of the

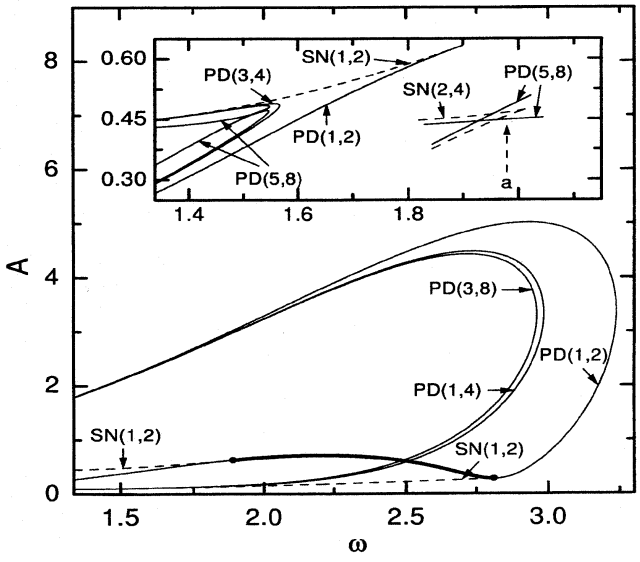

Fig. 2. Bifurcation structure associated with the first subharmonic resonance of the asymmetric fixed points z_a^*. The symbols PD and SN denote the period-doubling (solid line) and saddle-node (dashed line) bifurcation curves, respectively. Each curve is also labelled by a pair (p, q); p and q are the torsion number and period, respectively. For other details, see the text.

subharmonic resonance:

$$\mathrm{PD}(1,2) \to \mathrm{PD}(1,4) \to \mathrm{PD}(3,8) \to \cdots , \tag{5}$$

$$\mathrm{PD}(1,2) \to \mathrm{PD}(3,4) \to \mathrm{PD}(5,8) \to \cdots , \tag{6}$$

where the second PD route is shown in the inset.

We also note that the classification of the bifurcation curves by the period q and torsion number p is not unique, as is exemplified by the two different PD$(5,8)$ curves inside the PD$(3,4)$ curve (see the inset in Fig. 2). Both PD$(5,8)$ bifurcations are connected by an unstable orbit with period $q = 4$, which meets two SN$(2,4)$ bifurcations on its way to the other PD$(5,8)$ bifurcation. This can be read from a bifurcation diagram for the vertical cut at constant ω (e.g., see the cut "a" denoted by a dashed arrow). The SN$(2,4)$ curves lie in so close vicinity of the PD$(5,8)$ curves that they cannot be visible. We therefore give an artificial schematic pictogram which depicts the vicinity of the meeting point of the two PD$(5,8)$ curves more clearly in their topological structure. We also note that the structure inside the PD$(3,4)$ curve may be found in many other oscillators (refer to Fig. 7 in Ref. 18).

As shown in Fig. 2, two different SN$(1,2)$ curves touch the PD$(1,2)$ curve at the boundary points, denoted by the solid circles and decompose it into the supercritical and subcritical parts. The frequency values at the left and right boundary points are $\omega_{\mathrm{b,l}} \simeq 1.9$ and $\omega_{\mathrm{b,r}} \simeq 2.8$, respectively. The PD$(1,2)$ bifurcation is subcritical on the heavy part between the two boundary points, while it is supercritical on the other parts.

For a better understanding of the bifurcation structure in Fig. 2, we also present several bifurcation diagrams obtained by the amplitude scanning for a fixed frequency. We first consider the supercritical case of $\omega_{\mathrm{b,r}} < \omega < \omega_{\mathrm{f}}$. The bifurcation diagrams for $\omega = 3.0$, 2.97, and 2.95 are given in Figs. 3(a), 3(b), and 3(c), respectively. They show "period-bubblings". For $\omega = 3.0$, with increasing A the asymmetric fixed point z_{a}^{*} becomes unstable through a supercritical PD$(1,2)$ bifurcation, giving rise to the birth of a new stable period-doubled orbit. However, as A is further increased, it becomes restabilized via a reverse supercritical PD$(1,2)$ bifurcation by absorbing the newly-born period-doubled orbit. Consequently, a primary period-2 bubble is formed in the diagram, as shown in Fig. 3(a). With decreasing ω, this primary bubble bifurcates into secondary period-4 bubbles [see Fig. 3(b)], which also develop further higher-order bubbles, until fully-bloomed trees appear, as shown in Fig. 3(c). We note that, as A is increased periodic orbits are both created and destroyed, unlike the monotone behavior of the logistic map.[27] This kind of antimonotone behavior of the concurrent creation and destruction of periodic orbits has been observed in many other physical systems.[28]

We next consider the subcritical case of $\omega_{\mathrm{b,l}} < \omega < \omega_{\mathrm{b,r}}$, corresponding to the heavy part of PD$(1,2)$ curve in Fig. 2. An example for $\omega = 2.6$ is given in Fig. 4(a). Unlike the above supercritical case ($\omega_{\mathrm{b,r}} < \omega < \omega_{\mathrm{f}}$), the asymmetric fixed point z_{a}^{*} loses its stability through a subcritical PD$(1,2)$ bifurcation by absorbing an unstable asymmetric orbit of period 2 born via an asymmetric SN$(1,2)$ bifurcation. However,

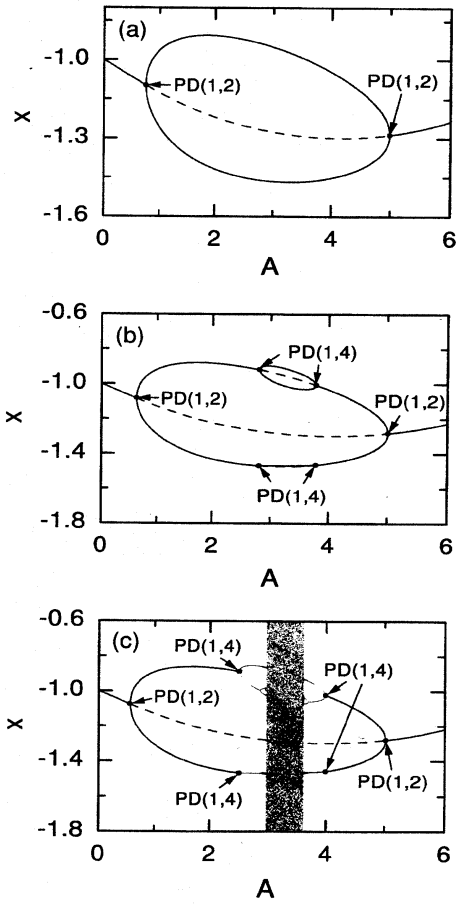

Fig. 3. Bifurcation diagrams (plot of x versus A) starting from a stable equilibrium point at $x = -1$ for (a) $\omega = 3.0$, (b) $\omega = 2.97$, (c) $\omega = 2.95$. They show "period bubblings". Here the solid line denotes a stable fixed point, while the dashed line represents an unstable fixed point. The symbols denote the same as those in Fig. 2.

as A is further increased, it becomes restabilized through a reverse supercritical PD(1, 2) bifurcation by absorbing the stable period-2 orbit born via the asymmetric SN(1, 2) bifurcation.

In the remaining range of $\omega_0 < \omega < \omega_{b,l}$ in Fig. 2, the asymmetric fixed point z_a^* becomes unstable through a supercritical PD(1, 2) bifurcation and a new stable orbit with period 2 appears. However, the fate of the newly-born period-2 orbit becomes different from the above supercritical case ($\omega_{b,r} < \omega < \omega_f$). An example for $\omega = 1.6$ is shown in Fig. 4(b). To show the topological structure more clearly, we also give the schematic pictogram of the bifurcation diagram in the inset. We note that the newly-born orbit with period 2 disappears at the upper SN(1, 2) bifurcation curve through the collision with an unstable period-2 orbit born at the lower SN(1, 2) bifurcation curve. The subsequent bifurcation behavior is similar to the above subcritical case ($\omega_{b,l} < \omega < \omega_{b,r}$). That is, with further increase of A,

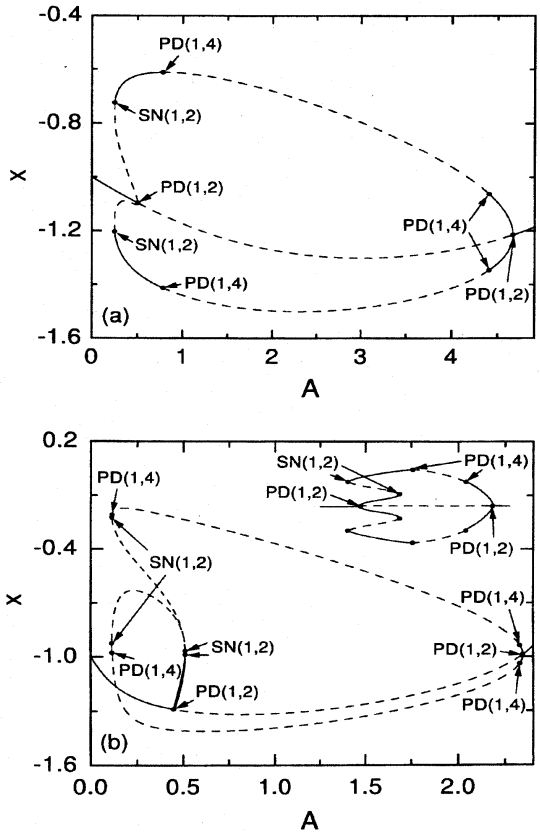

Fig. 4. Bifurcation diagrams (plot of x versus A) starting from a stable equilibrium point at $x = -1$ for (a) $\omega = 2.6$ (subcritical case), (b) $\omega = 1.6$ (supercritical case). Here the symbols and the line type denote the same as those in Figs. 2 and 3, respectively.

the asymmetric fixed point z_a^* becomes restabilized through a reverse supercritical PD(1, 2) bifurcation by absorbing the stable period-2 orbit born at the lower SN(1, 2) bifurcation curve.

3.2. *Bifurcation structure associated with the primary and superharmonic resonances*

With further decreasing ω from ω_0 $(= \sqrt{2})$, we continue to study the bifurcation structure associated with resonances of the asymmetric fixed point z_a^*. It is thus found that the frequency region may be divided into an infinity of subregions R_n $(n = 1, 2, 3, \ldots)$ with similar repeating bifurcation structures.

Each subregion R_n is associated with the nth-order resonance of the asymmetric fixed point z_a^*. As shown in Fig. 5(a), there exists the primary resonance horn with a cusp at $\omega \simeq \omega_0$ in the first subregion R_1 between $\omega \simeq 1.34$ and $\omega \simeq 0.66$. We note that a pair of SN(1, 1) bifurcation curves form the contour of the horn. Within this primary resonance, a secondary subharmonic response occurs at the

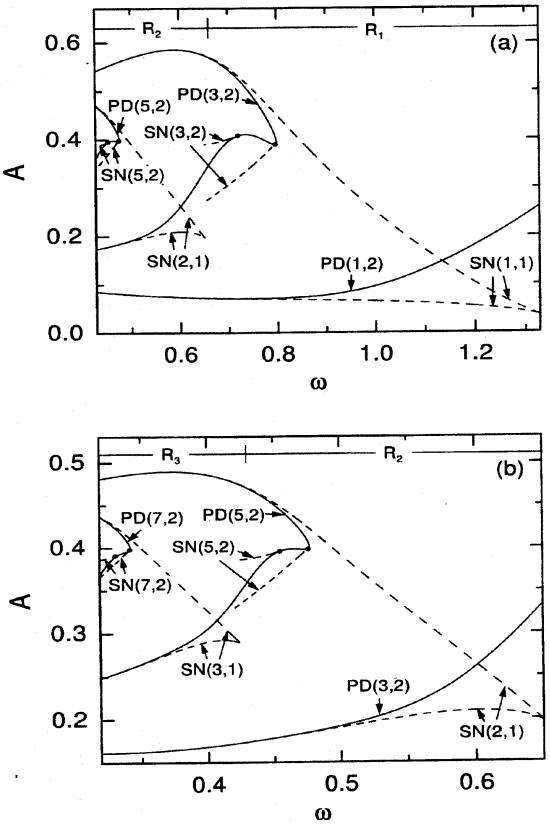

Fig. 5. Recurrence of self-similar resonance horns, associated with the primary and superharmonic resonances. The symbols denote the same as those in Fig. 2. For other details, see the text.

PD(3, 2) curve with a sharp nose at $\omega \simeq 0.8$. As in the case of the first subharmonic resonance explained in Subsec. 3.1, two SN(3, 2) curves touch the PD(3, 2) curves at the boundary points, labelled by the solid circles. Between these two boundary points, the PD(3, 2) bifurcation is subcritical and otherwise supercritical. These resonance horn and subharmonic resonance recur in a similar shape with decreasing ω. Figures 5(a) and 5(b) show a recurrent structure of the second and third resonance horns, corresponding to the superharmonic resonances of the second and third orders, and secondary subharmonic responses within them in the subregions R_2 and R_3. These resonance horns lean to the lower frequencies, which is a typical characteristic for the soft spring. We also note that recurrence of self-similar resonance horns occurs in many other driven oscillators such as the Toda, Morse, pendulum, and single-well Duffing oscillators.

In each subregion R_n, as the driving amplitude A is increased, the asymmetric fixed point z_a^* eventually disappears at the upper SN$(n, 1)$ curve through the collision with the unstable asymmetric fixed point born at the lower SN$(n, 1)$ curve. Moreover, in some subpart of R_n, subharmonic resonance occurs before the

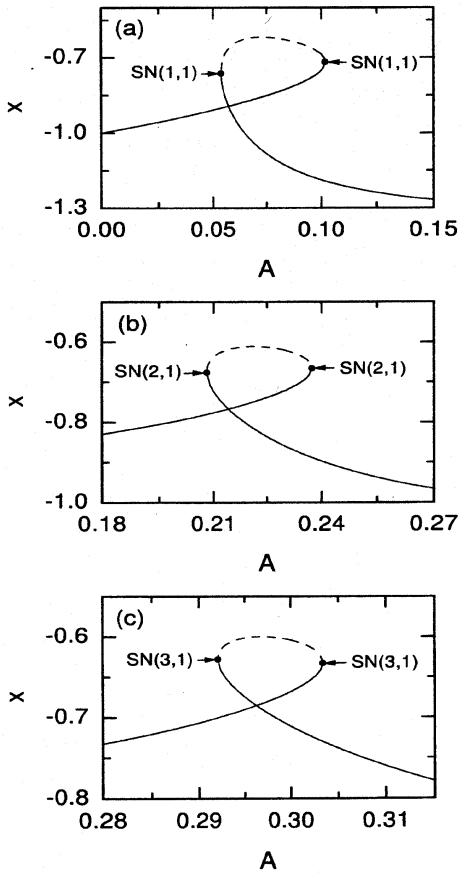

Fig. 6. Bifurcation diagrams (plot of x versus A) starting from a stable equilibrium point at $x = -1$ for $\omega = 1.2$, 0.62, and 0.415 are given in (a), (b), and (c), respectively. They show jump phenomena, associated with the primary and superharmonic resonances. Here the symbols and the line type denote the same as those in Figs. 2 and 3, respectively.

disappearance of z_a^*. As examples, we first consider the cases of $\omega = 1.2, 0.62$, and 0.415 without the subharmonic resonances. Three bifurcation diagrams for those cases are given in Figs. 6(a), 6(b) and 6(c), respectively. For each case, the asymmetric stable fixed point z_a^*, arising from $x = -1$, disappears through the SN$(n, 1)$ bifurcation by absorbing the unstable asymmetric fixed point born at the lower SN$(n, 1)$ bifurcation curve ($n = 1, 2, 3$). Then, a jump resonance occurs, in which z_a^* is replaced by the stable asymmetric fixed point z_{sn}^* born at the lower SN$(n, 1)$ bifurcation curve with torsion number n. The phase portrait of z_{sn}^* and its time evolution for some A are given in Fig. 7 (Figs. 7(a) and 7(b) for $\omega = 1.2$, Figs. 7(c) and 7(d) for $\omega = 0.62$, and Figs. 7(e) and 7(f) for $\omega = 0.415$). Note that with decreasing ω, the asymmetric periodic orbits z_{sn}^*, associated with the nth-order resonance, possesses an increasing number of loops (see the phase portraits in the left column). The waveform of x for $\omega = 1.2$ corresponds to the harmonic response, while the second and third waveforms for $\omega = 0.62$ and 0.415 correspond to the superharmonic

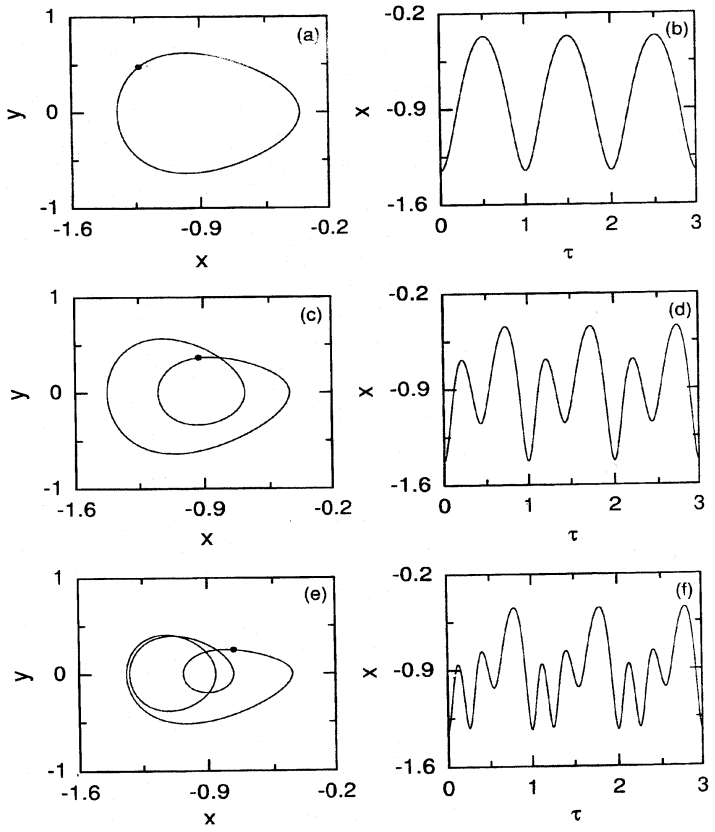

Fig. 7. Phase portraits (shown in the left column) and time evolutions $x(\tau)$ (shown in the right column. τ is a time normalized to the external driving period T $(= 2\pi/\omega)$, i.e., $\tau = t/T$) for $\omega = 1.2$ and $A = 0.12$ in (a) and (b), $\omega = 0.62$ and $A = 0.25$ in (c) and (d), and $\omega = 0.415$ and $A = 0.31$ in (e) and (f).

responses of second and third orders, respectively (see the time evolutions of x in the right column).

Finally, we discuss the subharmonic responses within the resonance horns. As shown in Fig. 5, there exists the PD$(2n+1,2)$ curve with a sharp nose within the SN$(n,1)$ resonance horn $(n = 1,2,3)$. Note that the bifurcation structures, associated with these secondary subharmonic resonances, are similar to the structure, associated with the first subharmonic resonance (see Fig. 2). That is, two SN$(2n+1,2)$ curves strike the PD$(2n+1,2)$ curve at the boundary points, denoted by the solid circles. The PD$(2n+1,2)$ bifurcation is subcritical on the part of the PD$(2n+1,2)$ curve between the two boundary points, whereas it is supercritical on the other parts. Thus, when crossing the lower part of the folded PD$(2n+1,2)$ curve, the stable asymmetric fixed point z_a^* becomes unstable via a subcritical or supercritical PD, while it becomes restabilized through a supercritical PD when crossing the upper part of the folded PD$(2n+1,2)$ curve. However, such a restabilized fixed point z_a^* eventually disappears at the upper SN$(n,1)$ curve.

4. Summary

We have made a detailed investigation of bifurcations associated with resonances of the asymmetric fixed points z_a^*, arising from the two stable equilibrium points of the potential, in the double-well Duffing oscillator. A phase diagram showing rich bifurcation structure, characterized by the bifurcation type (PD or SN), period q, and torsion number p, has been thus obtained in the $\omega - A$ plane. For the subharmonic resonances, the associated PD bifurcation curves become folded, along which there exist subcritical and supercritical parts. Diverse bifurcation phenomena such as period bubblings have been also observed. For the primary and superharmonic resonances, the associated SN bifurcation curves form horns, leaning to the lower frequencies. With decreasing ω, resonance horns with successively increasing torsion numbers repeat in a similar shape, as in many other driven oscillators such as the Toda, Morse, pendulum, and single-well Duffing oscillators. It is thus suggested that recurrence of self-similar resonance horns be a "universal" feature in the bifurcation structure of many driven nonlinear oscillators.

Acknowledgments

The author would like to thank W. Lim for his assistance in the numerical computation. This work was supported from the Interdisciplinary Research Program of the KOSEF under grant No. 1999-2-112-004-3 and the program of the Biomedlab Inc.

References

1. M. Lakshmanan and K. Murali, *Chaos in Nonlinear Oscillators: Controlling and Synchronization* (World Scientific, Singapore, 1996).
2. F. C. Moon, *Chaotic and Fractal Dynamics* (Wiley, New York, 1992), Secs. 6.2 and 7.7.
3. J. Guckenheimer and P. Holmes, *Nonlinear Oscillations, Dynamical Systems, and Bifurcations of Vector Fields* (Springer-Verlag, New York, 1983), Sec. 2.2.
4. P. J. Holmes, *Philo. Trans. R. Soc. London Ser.* **A292**, 419 (1979).
5. F. C. Moon and P. J. Holmes, *J. Sound Vib.* **65**, 275 (1979).
6. F. C. Moon, *ASME J. Appl. Mech.* **47**, 638 (1980).
7. R. A. Mahaffey, *Phys. Fluid* **19**, 1387 (1976).
8. F. C. Moon and G.-X. Li, *Phys. Rev. Lett.* **55**, 1439 (1985).
9. C. Holmes and P. Holmes, *J. Sound Vib.* **78**, 161 (1981).
10. F. T. Arecchi and F. Lisi, *Phys. Rev. Lett.* **49**, 94 (1982).
11. H. Ishii, H. Fujisaka and M. Inoue, *Phys. Lett.* **A116**, 257 (1986).
12. Y. H. Kao, J. C. Huang and Y. S. Gou, *Phys. Rev.* **A35**, 5228 (1987).
13. C. S. Wang, Y. H. Kao, J. C. Huang and Y. S. Gou, *Phys. Rev.* **45**, 3471 (1992).
14. W. Szemplinska-Stupnicka and J. Rudowski, Chaos **3**, 375 (1993).
15. V. Englisch and W. Lauterborn, *Phys. Rev.* **A44**, 916 (1991).
16. R. Gilmore and J. W. L. McCallum, *Phys. Rev.* **E51**, 935 (1995).
17. J. Guckenheimer and P. Holmes, *Nonlinear Oscillations, Dynamical Systems, and Bifurcations of Vector Fields* (Springer-Verlag, New York, 1983), p. 24.
18. U. Parlitz, *Int. J. Bif. Chaos* **3**, 703 (1993).
19. T. Kurz and W. Lauterborn, *Phys. Rev.* **A37**, 1029 (1988).

20. W. Knop and W. Lauterborn, *J. Chem. Phys.* **93**, 3950 (1990).
21. S.-Y. Kim and W. Lim (unpublished).
22. U. Parlitz and W. Lauterborn, *Phys. Lett.* **A107**, 351 (1985).
23. C. Scheffczyk, U. Parlitz, T. Kurz, W. Knop and W. Lauterborn, *Phys. Rev.* **A43**, 6495 (1991).
24. V. I. Arnold, *Ordinary Differential Equations* (MIT Press, Cambridge, 1973), p. 114.
25. J. Guckenheimer and P. Holmes, *Nonlinear Oscillations, Dynamical Systems, and Bifurcations of Vector Fields* (Springer-Verlag, New York, 1983), Sec. 3.5.
26. T. Uezu, *Phys. Lett.* **A93**, 161 (1983); P. Beiersdorfer, *ibid.* **A**, 379 (1984).
27. M. J. Feigenbaum, *J. Stat. Phys.* **19**, 25 (1978).
28. T. C. Newell, V. Kovanis and A. Gavrielides, *Phys. Rev. Lett.* **77**, 1747 (1996) and references therein.